
Application of the Liu and Murakami Damage Model for Creep Crack Growth Predictions in Power Plant Steels

Christopher J. Hyde, Wei Sun, Thomas H. Hyde,
Mohammed Saber and Adib A. Becker

Additional information is available at the end of the chapter

<http://dx.doi.org/10.5772/57052>

1. Introduction

Components in power plant, chemical plant, manufacturing processes, aero-engines, etc. may operate at temperatures which are high enough for creep to occur [1]. Such components may contain cracks or must be assumed to contain cracks as part of design life or remaining life analyses which are required [2]. In order to perform these analyses a number of approaches have been used, based on, for example, a fracture mechanics approach [3], or a continuum damage mechanics approach [4, 5, 6]. This paper is related to the use of the damage mechanics approach. In particular the methods used to obtain the material constants in the multiaxial form of the creep damage and creep strain equations are described. Most of the constants are obtained by fitting to uniaxial creep data; this is a well-established method [7]. However, in this paper, the determination of the multiaxial stress state parameter, α [8], is based on results from compact tension (CT) tests; this approach is novel and results in properties which are particularly suited for predicting creep crack growth in components, where the crack growth is defined by a damage parameter, ω . When this damage parameter reaches a critical value (0.99 chosen for the presented work) the material is regarded as 'completely damaged' and hence a void or crack growth is assumed to be present. A previously used technique for obtaining the multiaxial stress state parameter, based on the notch strengthening which usually occurs in Bridgman notch [9] creep rupture tests, relative to corresponding uniaxial tests, does not closely represent the stress states and constraint which occur at crack tips. The validity of the method proposed has been established by comparing finite element predictions of creep crack growth

in thumbnail cracked specimens with experimental data [7] using the material constants obtained from uniaxial creep and CT creep test results.

The material chosen for the investigation is a 316 stainless steel and a P91 steel because of the ready availability of uniaxial creep, uniaxial creep rupture, compact tension creep crack growth and thumbnail creep crack growth data at temperatures of 600°C and 650°C, respectively. The particular form of damage equation chosen for the investigation is that proposed by Liu and Murakami [6]. By comparison with the more commonly used Kachanov damage equations [4], it was found that the Liu and Murakami equations do not cause the time steps in the finite element analyses to become impractically small [10] and unlike the Kachanov equations, they produce results which are relatively insensitive to element size near the crack tip. These aspects are covered further in the paper.

2. Experimental testing

Two materials have been used for the experimental testing presented, namely P91 steel and 316 stainless steel. The modified 9Cr (P91) steel was initially developed in the US in the early 1980s and was introduced to UK power plants in the early 1990s, to replace some of the components made from low alloy ferritic steels, as its high creep strength allows the use of thinner walled components, which will be less prone to thermal fatigue cracking. The 316 stainless steel is also a creep resistant steel, which is widely used in power plants at high temperature. Table I shows the chemical composition of the P91 steel and 316 stainless steel. All tests for P91 were performed at 650°C [11] and all tests for 316 stainless steel were performed at 600°C [10].

	Cr	Ni	Mo	Mn	Si	Cu	V	Co	S	C	Nb	N	Fe
P91	8.74	-	0.98	0.36	0.022	0.08	0.21	-	-	0.11	0.12	0.048	Balance
316	16.8	11.8	2.15	1.42	0.5	0.49	0.08	0.07	0.03	0.02	0.02	-	Balance

Table 1. Chemical composition (wt %) of P91 and 316 Stainless Steel

Three main specimen types have been used in order to obtain the experimental data shown in this paper, namely, uniaxial specimens, compact tension (CT) crack growth and thumbnail crack growth creep specimens, as shown in Figure 1, Figure 2 and Figure 3, respectively. Testing was also carried out using side-grooved CT specimens (see Figure 4) for P91. Tunnelling behaviour was observed for the plain specimens and relatively uniform creep crack growth fronts were observed for the side grooved specimens.

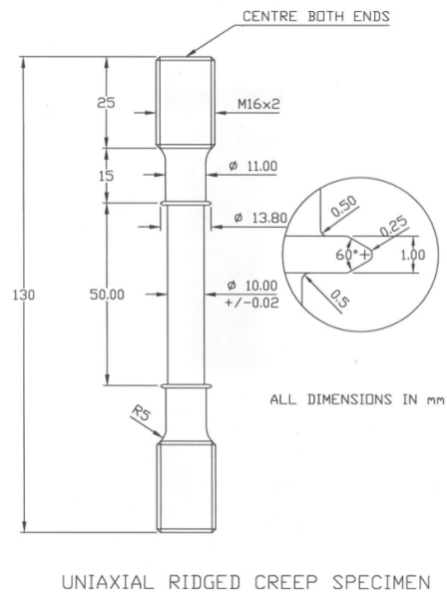


Figure 1. Uniaxial creep specimen geometry (dimensions in mm).

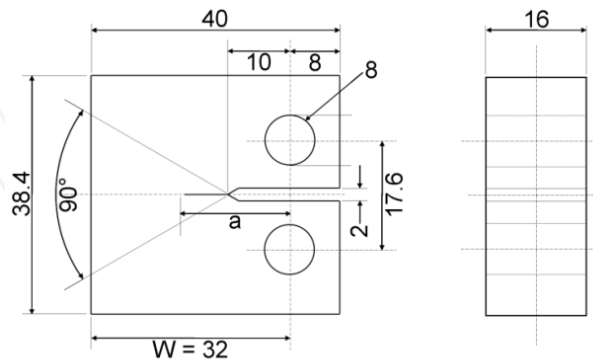


Figure 2. CT specimen geometry (dimensions in mm).

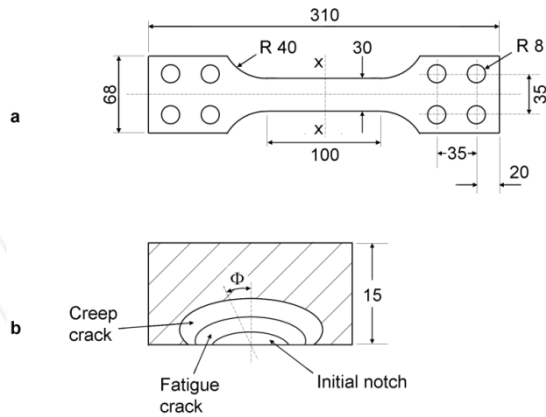


Figure 3. Thumbnail crack specimen (a) geometry, and (b) crack profile (dimensions in mm).

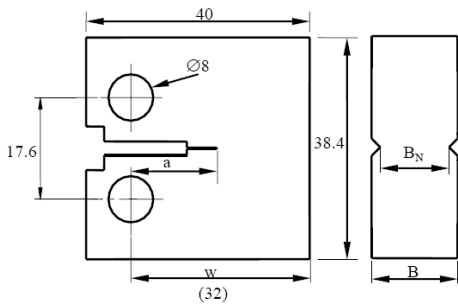


Figure 4. Side-grooved CT specimen (dimensions in mm).

3. Liu and Murakami creep damage model

3.1. Definition of the model

The governing equations for the Liu and Murakami creep damage model are shown by equations (1), (2) and (3).

$$\dot{\varepsilon}_{eq}^c = \frac{3}{2} A \sigma_{eq}^n \frac{S_{ij}}{\sigma_{eq}} \exp \left(\frac{2(n+1)}{\pi \sqrt{1+3/n}} \cdot \left(\frac{\sigma_1}{\sigma_{eq}} \right) \cdot \omega^{3/2} \right) \quad (1)$$

$$\dot{\omega} = B \frac{(1 - e^{-q_2})}{q_2} \sigma_r^\chi e^{q_2 \omega} \quad (2)$$

$$\sigma_r = \alpha \sigma_1 + (1 - \alpha) \sigma_{eq} \quad (3)$$

where A , n , B , q_2 and χ are material constants. σ_r is the rupture stress, ε_{eq}^c and σ_{eq} are the equivalent strain and equivalent stress, respectively, σ_1 is the maximum principle stress, S_{ij} is the deviatoric stress and ω is the damage variable [10]. When the damage value reaches a critical value (0.99 within the present work), crack growth is assumed to have occurred into the regions where this has happened. The derivation of the uniaxial form of these equations can be seen in [10].

3.2. Determination of the material constants

The required material constants shown in equations (1) and (2), i.e. A , n , B , χ and q_2 , can be determined from uniaxial creep data as detailed in [12] and a creep tip relevant value of the multiaxiality constant, α , can be determined from CT creep crack growth data as detailed in [10].

3.2.1. Uniaxial constants

From equation (1) the relationship between the minimum strain rate and stress can be given by [10]:

$$\log(\dot{\varepsilon}^c) = n \log(\sigma) + \log(A) \quad (4)$$

Therefore, using experimental uniaxial creep data to plot $\log(\dot{\varepsilon}^c)$ vs. $\log(\sigma)$ and fitting a straight line of best fit through this data allows the identification of n from the gradient and A from the y-axis intercept. An example of this plot is shown in Figure 5, for 316 stainless steel, at 600°C. From equation (2) [10]:

$$\log(t_f) = -\chi \log(\sigma) + \log\left(\frac{1}{B}\right) \quad (5)$$

Therefore, plotting $\log(t_f)$ vs. $\log(\sigma)$ using data obtained from uniaxial experiments, allows the identification of both χ , from the gradient of the straight line of best fit and B , from the y-intercept. Figure 6 shows an example of this plot for uniaxial, 316 stainless steel data at 600°C.

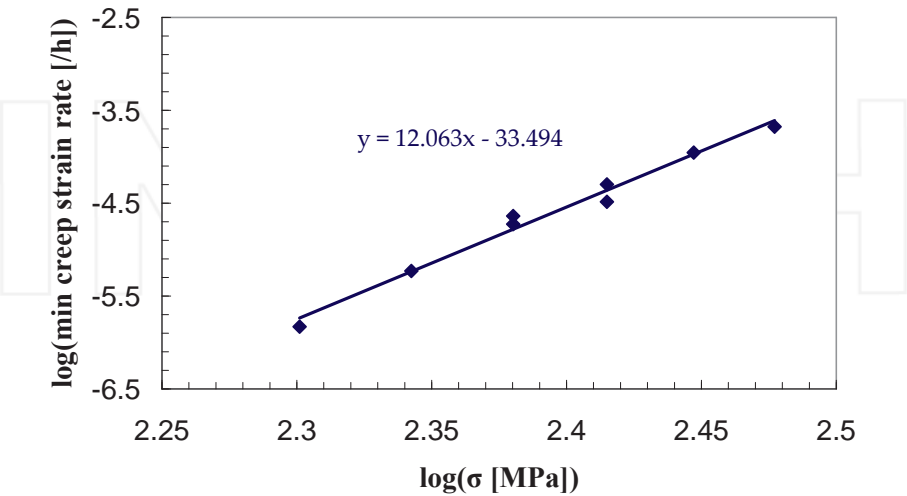


Figure 5. Linear fit to creep strain rate vs. σ on a log-log scale for 316 stainless steel at 600°C.

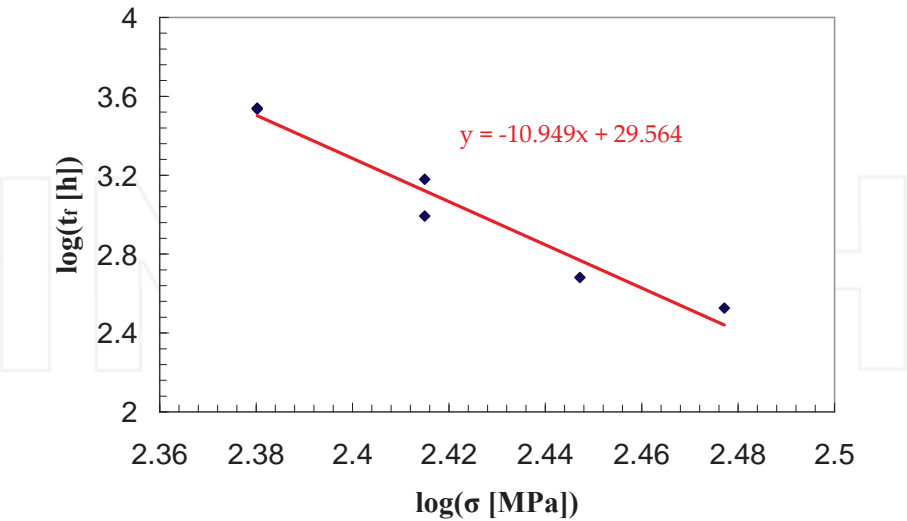


Figure 6. Linear fit to $\log(t_r)$ vs. $\log(\sigma)$ for 316 stainless steel at 600°C.

In order to obtain q_2 , a curve fitting process is used on the ε^c vs. time data in order to determine the value of q_2 which is the optimum fit at all stress levels. In order to plot ε^c vs. time using the model, ε^c must first be found as a function of t [10]. This equation is as follows:

$$\dot{\varepsilon}^c = A\sigma^n \exp \left(\frac{2(n+1)}{\pi \sqrt{1+3/n}} \cdot \left(-\frac{\ln(1-B(1-e^{-q_2})\sigma^z t)}{q_2} \right)^{3/2} \right) \quad (6)$$

An example of this plot using uniaxial creep data for 316 stainless steel, at 600°C, is shown by Figure 7.

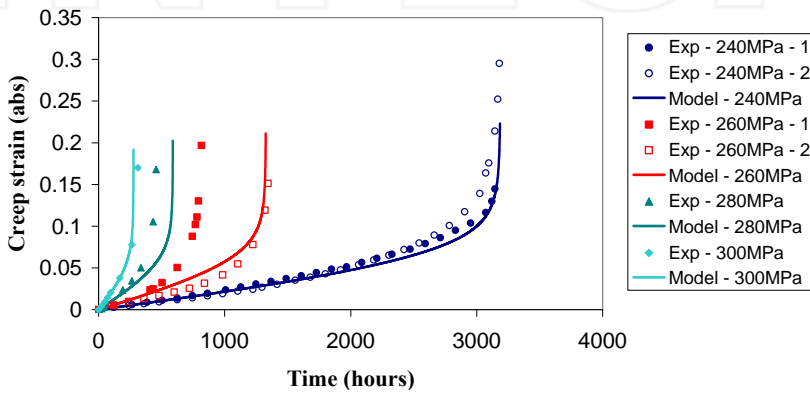


Figure 7. Comparison of the Liu and Murakami creep damage model to uniaxial, experimental creep data for 316 stainless steel at 600°C.

3.2.2. Multiaxiality parameter, α

Equation (3) is used for the rupture stress, σ_r , within the model to include the multiaxial stress effect. Within this equation is the material constant, α , which is not required for the uniaxial condition. However, if a multiaxial stress condition exists, the α value is required. It can be obtained from equation (2) that [10]:

$$t_f = \frac{1}{B(\alpha\sigma_1 + (1-\alpha)\sigma_{eq})^z} \quad (7)$$

It can therefore be seen that the failure time is dependent on this multiaxial constant, α . Therefore, experimental data can be used in order to obtain the value of α . A series of finite

element (FE) modelling of the conditions of the experimental tests are then carried out using the material properties (A , n , B , χ , and q_2) obtained from the corresponding uniaxial test data, together with a different α -value for each calculation. The α -value which results in the same failure time as that of the experimental test is taken to be the material α -value. The average α -value for a range of load levels applied in the experiments gives a more accurate estimate for the α -value. The process is capable of giving α -values which can be used with confidence when the triaxial stress state within the specimen is similar to that in the components for which damage zones and failure times are to be determined. Therefore for a crack tip (crack growth) condition, crack growth experimental data is used. A series of FE calculations, to predict the creep crack growth in the experimental CT specimens, as shown in Figure 8, were carried out for the experimental test durations, using the same load levels. The results of the time to the final crack length measured in an experimental test are plotted against α , and the experimental value of time to this given crack length, t_a , used to interpolate for the material α value. An example of this plot for a 316 stainless steel CT specimen geometry subjected to a load of 7.48kN, at 600°C, is shown by Figure 9. The application of the experimental t_a -value and reading of the material α -value is indicated by the dashed line.

3.3. Material constants

The material constants obtained for P91 and 316 stainless steels are given in Table 2.

	A	n	B	χ	q_2	α
P91	1.09×10^{-20}	8.462	2.95×10^{-16}	6.789	3.2	0.313
316	1.47×10^{-29}	10.147	2.73×10^{-30}	10.949	6.35	0.478

Table 2. Material Constants in Damage Equations for P91 at 650°C and 316 Stainless Steel at 600°C (σ in MPa and t in h).

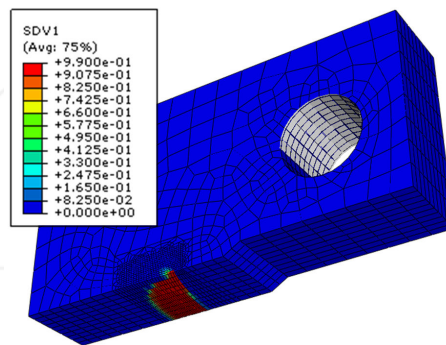


Figure 8. CT specimen FE mesh.

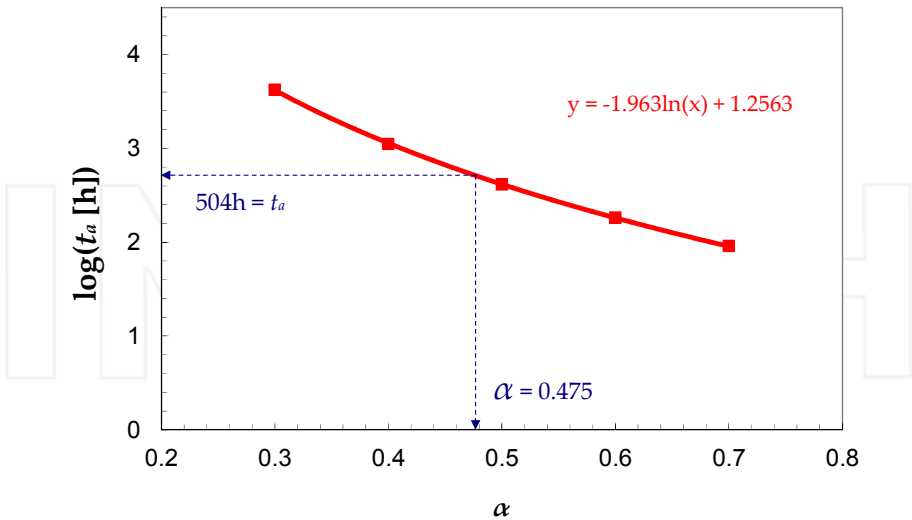


Figure 9. Typical α determination graph for 316 stainless steel from CT test data, using a logarithmic fitting.

3.4. Predictive capability of the model

3.4.1. P91 at 650°C

A typical three-dimensional FE mesh and 0.99 damage (crack) zone for the CT specimen geometry is shown in (plain CT specimen), where due to two planes of symmetry in a CT specimen, only one quarter of the specimen has been modelled, with the appropriate boundary conditions applied [11]. Testing and modelling has been carried out for P91 at 650°C for both plain and side-grooved CT specimens (see Figure 2 and Figure 4), with the model constants being calculated as shown in section 3.2. Figure 10 shows an example of a tested CT specimen of each type and shows the difference in the corresponding characteristic crack front shapes. Examples of FE creep crack growth modelling of P91 CT specimens using the damage mechanics approach are illustrated in Figure 10 and Figure 11. Figure 10 shows the damage contours, at times close to fracture, of a plain specimen and a side-grooved specimen. It can be seen from Figure 10 that the tunnelling effect observed in the plain specimens and the essentially uniform crack growth observed in the side-grooved specimens, as shown in Figure 10, have been reasonably accurately reproduced by the FE analyses. In addition and more importantly, as can be seen in Figure 11, the FE damage modelling has reasonably accurately predicted the creep crack growth behaviour for the P91 CT specimens, when compared with the corresponding experimental results.

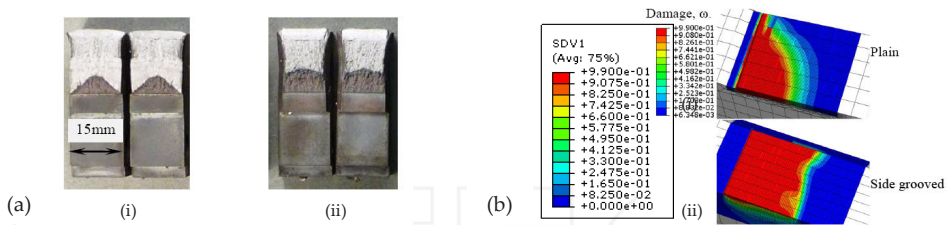


Figure 10. Examples of creep profiles for P91 at 650°C at times close to failure (a) Experimental CT specimen photographs and (b) FE damage contours [(i) plain ($P = 5\text{ kN}$) and (ii) side-grooved ($P = 3.6\text{ kN}$)].

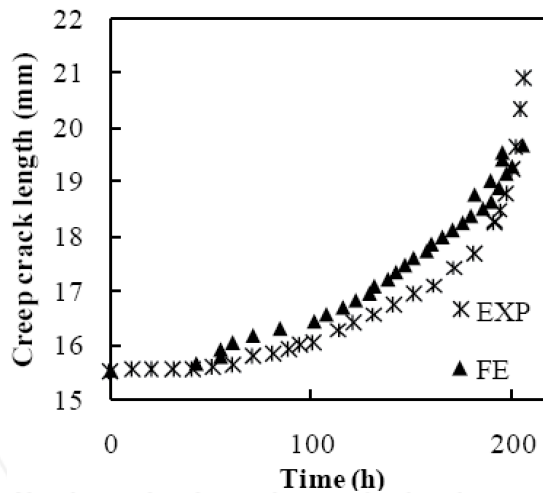


Figure 11. Predicted creep crack growth compared to experimental results for a P91 CT specimen (side-grooved, $P = 3.6\text{ kN}$).

3.4.2. 316 stainless steel at 600°C

The comparisons of the experimental and FE creep crack growths for three plain CT specimens, each subjected to a different test load, are shown in Figure 12, from which it can be seen that the crack front shapes, as well as the extents of creep crack growth, were accurately predicted.

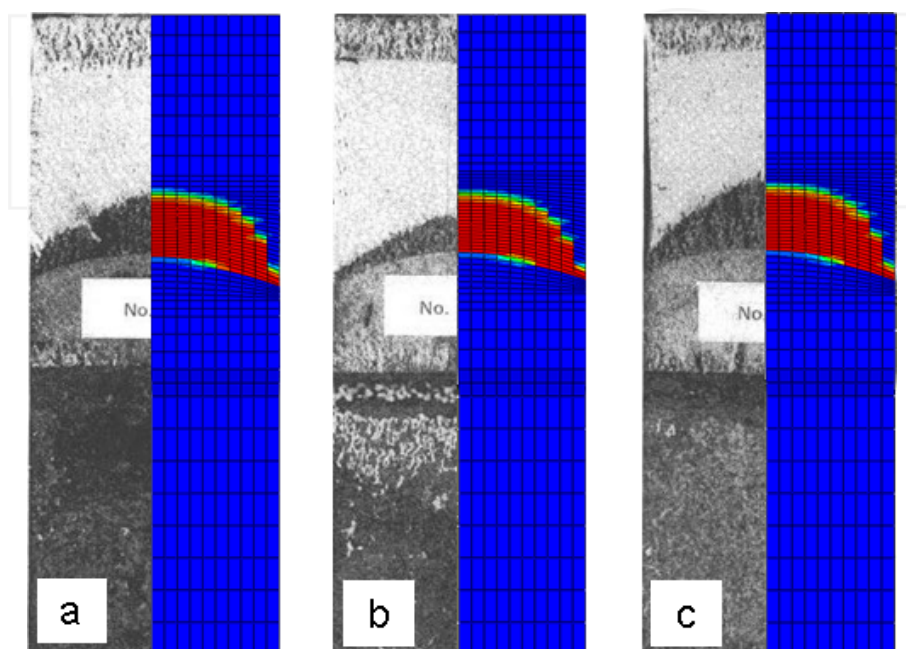


Figure 12. Tested specimen photo to FE damage contour comparisons (a) 8.522kN (b) 6.977kN (c) 7.476kN.

As the multiaxial constant, α , was determined using the CT crack growth data, it is to some extent not surprising that the FE crack growth predictions correspond well to this experimental data, with all of the other material constants having been determined using data from uniaxial creep data. However, similar simulations have been performed for thumbnail crack geometries using the same constants as for the CT specimen and can therefore be considered as 'pure prediction'. Figure 13 shows an example of the 3-dimensional mesh (and 0.99 damage (crack) zone) used for the thumbnail crack growth simulations. As with the CT specimens, due to two planes of symmetry in a thumbnail crack specimen, only one quarter of the specimen has been modelled, with the appropriate boundary conditions applied [10].

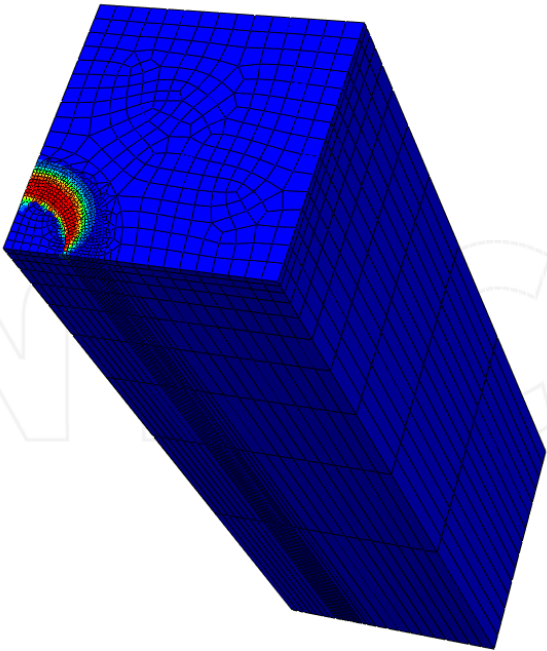


Figure 13. thumbnail crack specimen FE mesh.

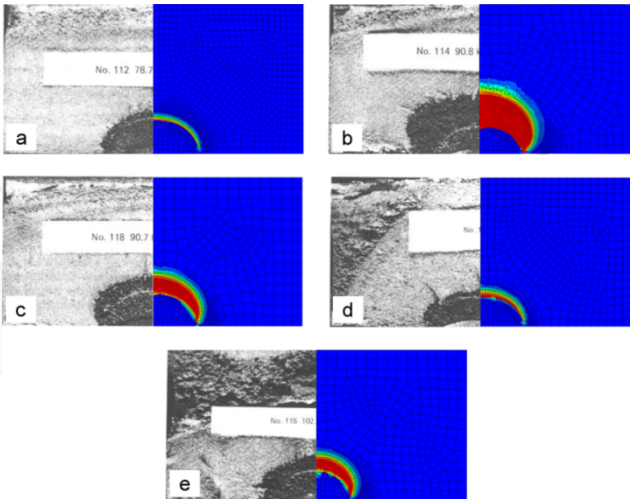


Figure 14. Tested specimen photo to FE damage contour comparisons (a) 78.7kN (b) 90.8kN (c) 90.7kN (d) 91.7kN (e) 102.3kN.

The comparisons of the experimental and FE creep crack growths for five thumbnail specimens, each subjected to a different test load, are shown in Figure 14, from which it can be seen that similarly to the CT predictions, the crack front shapes, as well as the extents of creep crack growth were accurately predicted.

4. Discussion and future work

A comprehensive procedure for the determination of the material constants for the Liu and Murakami creep damage model, based on experimental data, has been described. Particular attention has been given to ensuring a constant of multiaxiality value (α) which is highly appropriate to crack tip conditions. These constants have been applied, for a 316 stainless steel at 600°C and a P91 steel at 650°C, to a user subroutine for the Liu and Murakami model which has been used in conjunction with Finite Element package ABAQUS, in order to provide numerical predictions for creep crack growth in both compact tension specimen and thumbnail specimen geometries. Comparisons of the model predictions to corresponding experimental data for multiple specimen geometries, in terms of both crack growth and final crack length/profile, show extremely close correlation.

Also shown is the effect that side-grooves have on the crack profile in a CT specimen and the ability of the Liu and Murakami creep damage model to predict this more uniform crack profile observed in side-grooved CT specimens.

Nomenclature

Roman symbols

A Liu and Murakami Creep Law Coefficient

B Liu and Murakami Creep Law Coefficient

n Liu and Murakami Creep Law Constant

P Load

q_2 Liu and Murakami Creep Law Constant

S_{ij} Deviatoric Stress

t_a Time to Crack Length, a

t_f Failure Time

T Temperature

Greek symbols

α Multiaxiality Constant

$\dot{\epsilon}_{eq}^c$ Equivalent Creep Strain Rate

σ_{eq} Equivalent Stress

σ_r Rupture Stress

σ_1 Maximum Principal Stress

χ Liu and Murakami Creep Law Constant

ω Damage

Abbreviations

CT Compact Tension

FE Finite Element

Acknowledgements

The authors would like to thank Dennis Cooper, Brian Webster and Shane Maskill for their assistance with the experimental work.

Author details

Christopher J. Hyde^{1*}, Wei Sun¹, Thomas H. Hyde¹, Mohammed Saber² and Adib A. Becker¹

*Address all correspondence to: christopher.hyde@nottingham.ac.uk

1 Department of Mechanical, Materials and Manufacturing Engineering, University of Nottingham, Nottingham, UK

2 Department of Production and Mechanical Design, Faculty of Engineering, University of Port Said, Port Said, Egypt

References

- [1] R. K. Penny and D. L. Marriott, "Design for Creep", McGraw-Hill, Liverpool, 1971.
- [2] T. H. Hyde, W. Sun and A. A. Becker, "Creep crack growth in welds: A damage mechanics approach to predicting initiation and growth of circumferential cracks in CrMoV weldments", *Int. J. Pres. Ves. & Piping*, 2001; 78, 765-771.
- [3] B. Dogan and B. Ptrowski, "Creep crack growth of high temperature weldment." *International Journal of Pressure Vessel and Piping*, 2001, 78, 795-805.

- [4] L. M. Kachanov, "The time to failure under creep condition", *Izv. Akad. Nauk., SSSR. Tekh. Nauk*, 1958, 8, 26-31.
- [5] Y. N. Robotnov, "Creep Problems of Structural Members", *North-Holland*, 1969.
- [6] Y. Lui and S. Murakami, "Damage localization of conventional creep damage models and proposition of a new model for creep damage analysis", *JSME International Journal*, 1998, 41, 57-65.
- [7] T. H. Hyde, "Creep crack growth in 316 stainless steel at 600°C", *High Temperature Technology*, 1988, 6(2), 51-61.
- [8] D. R. Hayhurst and C. J. Morrison, "Development of continuum damage in the creep rupture of notched bars", *Phil. Trans. R. Soc. Lond. (A)*, 1984, 311, 103-129.
- [9] G. A. Webster, S. R. Holdsworth, M. S. Loveday, I. J. Perrin, K. Nikbin, H. Purper, R. P. Skelton, and M. W. Spindler, "A code of practice for conducting notched bar creep rupture tests and for interpreting the data", *J. Fatigue and Fatigue of Eng. Materials and Struct.*, 2004, 24, 319-342.
- [10] C. J. Hyde, T. H. Hyde, W. Sun and A. A. Becker, "Damage mechanics based predictions of creep crack growth in 316 stainless steel", *Engineering Fracture Mechanics*, 2010, 77(12), 2385-2402.
- [11] T. H. Hyde, M. Saber and W. Sun, "Testing and modelling of creep crack growth in compact tension specimens from a P91 weld at 650°C," *Engng. Frac. Mech.*, 2010, 77(15), 2946-2957.
- [12] T. H. Hyde and W. Sun, "Determining high temperature properties of weld materials," *JSME Int. J. of Solids Mechanics & Material Eng, Series A*, 2000, 43(4), 408-414.

INTECH

